BIOFOULING, 2018
VOL. 34, NO. 3, 335–345
https://doi.org/10.1080/08927014.2018.1440392

Taylor & Francis
Taylor & Francis Group

Check for updates

Agent-based model of diffusion of N-acyl homoserine lactones in a multicellular environment of *Pseudomonas aeruginosa* and *Candida albicans*

Gael Pérez-Rodríguez[a,b], Sónia Dias[c,d], Martín Pérez-Pérez[a,b], Florentino Fdez-Riverola[a,b], Nuno F. Azevedo[e] and Anália Lourenço[a,b,f]

[a]ESEI – Escuela Superior de Ingeniería Informática, Universidad de Vigo, Ourense, Spain; [b]CINBIO - Centro de Investigaciones Biomédicas, University of Vigo, Vigo, Spain; [c]ESTG - Instituto Politécnico de Viana do Castelo, Viana do Castelo, Portugal; [d]LIAAD-INESC TEC, University of Porto, Porto, Portugal; [e]LEPABE – Department of Chemical Engineering, Faculty of Engineering, University of Porto, Porto, Portugal; [f]CEB - Centre of Biological Engineering, University of Minho, Braga, Portugal

ABSTRACT

Experimental incapacity to track microbe–microbe interactions in structures like biofilms, and the complexity inherent to the mathematical modelling of those interactions, raises the need for feasible, alternative modelling approaches. This work proposes an agent-based representation of the diffusion of N-acyl homoserine lactones (AHL) in a multicellular environment formed by *Pseudomonas aeruginosa* and *Candida albicans*. Depending on the spatial location, *C. albicans* cells were variably exposed to AHLs, an observation that might help explain why phenotypic switching of individual cells in biofilms occurred at different time points. The simulation and algebraic results were similar for simpler scenarios, although some statistical differences could be observed ($p < 0.05$). The model was also successfully applied to a more complex scenario representing a small multicellular environment containing *C. albicans* and *P. aeruginosa* cells encased in a 3-D matrix. Further development of this model may help create a predictive tool to depict biofilm heterogeneity at the single-cell level.

ARTICLE HISTORY
Received 7 November 2017
Accepted 8 February 2018

KEYWORDS
Cellular systems; quorum-sensing signalling; agent-based modelling; three-dimensional model representation; individual molecule simulation

Introduction

In biofilms, microorganisms are embedded in a heterogeneous three-dimensional matrix, and the steep chemical or physical gradients that can be found within this matrix imply that isogenic cells often display different phenotypes (Flemming et al. 2016; Gao et al. 2016). While a few studies provide preliminary insights into this intercellular heterogeneity (eg Tsimring; Carnes et al. 2010; Stiegelmeyer and Giddings 2013; Trovato et al. 2014; Yu 2014), it is still complex and time-consuming to understand and predict the behaviour of individual cells in a spatially structured consortium.

One common example of cellular heterogeneity in biofilms is observed when *Pseudomonas aeruginosa* and *Candida albicans* form mixed species biofilms. *C. albicans* and *P. aeruginosa* are commonly found together in the lungs of cystic fibrosis patients and both microorganisms frequently infect immunocompromised individuals (Trejo-Hernández et al. 2014; Fourie et al. 2016). Under certain host circumstances, some of the *C. albicans* cells alter their morphology from yeast to hyphal and are able to invade epithelial cells and cause tissue damage (Sudbery 2011).

Morphological transition in *C. albicans* is mediated by a wide range of phenomena, from environmental factors to molecular cues (Peleg et al. 2010). One of those cues is 3-oxo-C(12)-homoserine lactone, a compound that belongs to the well-known class of quorum-sensing molecules named N-acyl homoserine lactones (AHLs) (Méar et al. 2013; Fourie et al. 2016). This AHL is secreted by *P. aeruginosa* and is known to inhibit hyphal development at concentrations of 200 μM (Hogan et al. 2004). While it is possible to quantify the percentage of *C. albicans* cells that are able to do the transition in a mixed species biofilm, no current method provides further understanding of why some cells undergo the transition while others do not. One hypothesis is that the different phenotypes are somewhat related to the different localisation of the cells in the biofilm (Alberghini et al. 2009). For instance, it would be expected that the *C. albicans* cells that are closer to the *P. aeruginosa* cells (and hence, more immediately exposed to a higher concentration of AHLs) would transition more slowly.

CONTACT Anália Lourenço analia@uvigo.es
Supplemental data for this article can be accessed here.

© 2018 Informa UK Limited, trading as Taylor & Francis Group

The aim of this study was to demonstrate the usefulness of agent-based modelling (ABM) to predict morphological transitions in mixed species biofilms. The *C. albicans* and *P. aeruginosa* multicellular environment was used as a proof-of-concept to study, in future, quorum sensing (QS) in biofilms. For the simplest scenarios, where one *P. aeruginosa* cell would be in the presence of one *C. albicans* cell, ABM results were compared against results obtained by an algebraic approach. The final model represents a mixed population of *C. albicans* and *P. aeruginosa* cells, where fungal cell transition to the hyphal form depends on a pre-established, experimentally observed threshold of AHL molecules reaching the fungal cell.

Materials and methods

Agent-based model of AHL diffusion in multicellular environments

The proposed model describes a mixed population of *C. albicans* and *P. aeruginosa* cells. Moreover, it describes the secretion of AHL molecules by the bacterial cells and the diffusion of such molecules until collision with *C. albicans* or the simulation boundaries occurs. The characteristics of both cell types and the molecules are described in Tables 1 and 2.

Spherical approximation is a typical, effective way to create a realistic and computer tractable representation of molecules (Feig and Sugita 2013). In particular, the excluded volume, which is approximated by the hydrodynamic or Van der Waals radius, is a good measurement of the actual space occupied by molecules (Kalwarczyk et al. 2012). This volume accounts for the purely structural dimensions of the molecules as well as the interactions with the solvent medium. Using this approach, the radius of each particle was calculated using Equation 1:

$$r = 0.0515 \times M_w^{0.392}(nm) \quad (1)$$

where M_w corresponds to the molecular weight of the molecule.

The diffusion coefficient for the AHL was calculated using the Stokes–Einstein equation for the diffusion of spherical particles in a liquid (see Equation 2):

$$D_c = \frac{k_B \times T}{6 \times \pi \times \eta \times r} \quad (2)$$

where k_B is the Boltzmann's constant, T is the absolute temperature, η is the viscosity of the medium, and r is the hydrodynamic radius of the spherical particle. The value of viscosity was considered to be similar to water at 37°C, as biofilms are composed by 70–95% of water (Flemming 1993). Moreover, a formerly established equivalence between time and time steps, ie 1 time step = 2.05E-9 s, was considered (Pérez-Rodríguez et al. 2016).

Agent-based simulations studied the impact of spatial location over cell phenotypic switching. Simulations included multiple scenarios of cell distribution and each simulation was replicated six times. For simplicity, the simulation environment was dimensioned to fit the population of cells studied in each group of simulations (ie cell volume times the number of cells) and a minimal volume of extracellular space (ie a realistic spacing between the cells).

At the beginning of the simulation, each *P. aeruginosa* cell secreted 5,000 AHL molecules. Depending on the simulation volume and the number of cells releasing AHLs, the number of molecules corresponded to a concentration of ~ 1–10 nM, which is in accordance with the concentration of AHLs typically estimated in microbial cultures (Hogan et al. 2004). Furthermore, the diffusion of the AHL molecules was implemented as a perpendicular movement to the surface of the *P. aeruginosa* cells, and those molecules that reached the simulation boundary would leave the environment. When possible, simulations results were compared against a mathematical model to verify the coherence of the ABM.

The first group of simulations analysed the effect of the distance *d* between *C. albicans* and *P. aeruginosa* cells. The volume of the simulation environment was 1,531–2,040 μm^3, and included one fungal cell and one bacterial cell, aligned in an imaginary x-axis. The underlying assumption was that the percentage of AHL molecules reaching the *C. albicans* cell would depend on the distance between both cells, ie the closer the *P. aeruginosa* cell is to the *C. albicans* cell, the more AHL molecules would reach *C. albicans*.

The second group of simulations studied the impact of the number of cells as well as their orientation and localisation over cell communication. The volume of the simulation environment was 1,633–6,226 μm^3. The comparison of simulation results was based on the percentage of AHL

Table 1. Basic agent properties and interaction rules in QS simulations.

Agent	Geometrical shape	Initial number	Interaction rules
C. albicans	Sphere	1–2*	Perceives AHL signals and, if reaching threshold, blocks hyphal transition
P. aeruginosa	Spherocylinder	1–5*	Secretes AHL molecules
AHL	Sphere	0–25,000*	'Detects' *C. albicans* as a signal receptor

*Number varied according to the purposes of each simulation scenario, as detailed in the text.; Agent characterisation includes geometrical shape, number of agents at the beginning of simulation, and interaction rules.

Table 2. Biological information needed for QS simulations.

Agent	Molecular weight (g mol^{-1})	Radius (μm)	Height (μm)	Diffusion rate (μm^2 s^{-1})	References
C. albicans	–	5	–	–	Klis et al. (2014)
P. aeruginosa	–	0.5	3	–	Karupiah and Chaudhri (2004)
AHL	227.3	4.32E-5	–	7.60E-9	Winson et al. (1995)

Notes: Experimental and calculated information includes molecular weight, geometrical metrics and, whenever applicable, diffusion rate. The shape and size of the microorganisms is an approximation, as it is well known that it depends on a wide range of environmental factors.

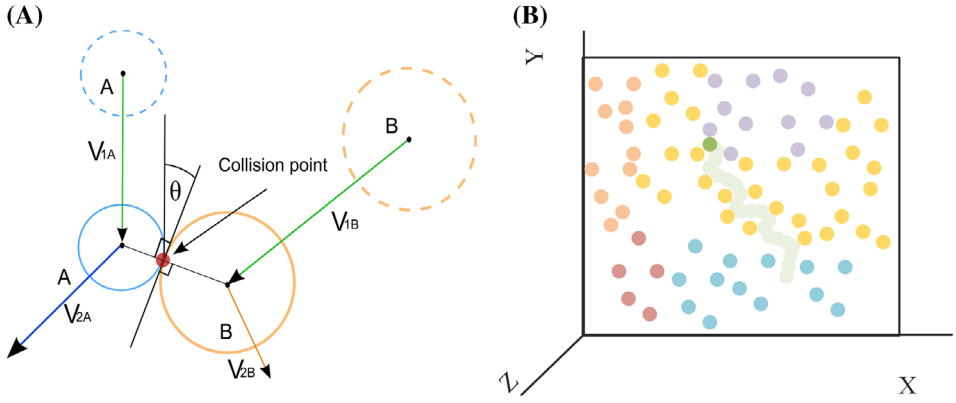

Figure 1. (A) Collision detection and resolution. V_{1A} and V_{1B} stand for the initial velocity vectors of molecules A and B whilst V_{2A} and V_{2B} represent the velocity vectors after collision. At the collision point, there is the deflection angle θ between the normal and the actual velocity vector of each agent; (B) example of Brownian motion in a crowded environment. Brownian movement of the green molecule emerges naturally by colliding with other molecules in the environment.

molecules that reached the *C. albicans* cell as well as the time that the individual molecules took to reach the cell.

The third group of simulations addressed the influence of environment feeding, ie AHL molecules produced by bacterial cells outside the observed vicinity. The aim was to evaluate the effect of cell localisation and molecular diffusion in morphological switching, under the assumption that both cell vicinity and the overall distribution of the cell population play a part in reaching the switching threshold. The volume of the simulation environment was 1,939 μm^3. *P. aeruginosa* secreted 5,000 AHL molecules, maintaining previous simulation conditions, and the environment released 600 AHL molecules, with a random direction, at every 10,000 time steps. The number of AHL molecules released by the environment was kept low, notably they were not all released at the beginning of the simulation, in order to keep to the above-mentioned concentrations of 1–10 nM.

Finally, the diffusion of AHLs within a multicellular environment was simulated. The volume of the simulation environment was 13,518 μm^3, including two *C. albicans* cells and five *P. aeruginosa* cells. Cells were randomly distributed and the *P. aeruginosa* cells were kept parallel to the y-axis. Depending on the spatial location, *C. albicans* cells were variably exposed to AHL molecules. The threshold for *C. albicans* morphological transition was set to 2,000 AHL molecules colliding with the cell. As there were no experimental values regarding the number of molecules that inhibit hyphal development (only concentrations were known), this threshold was selected as a surrogate value that differentiates the behaviour of two *C. albicans* cells when exposed to the same, experimentally validated concentration of AHLs.

The multi-agent simulator of neighbourhoods (MASON) framework supported the simulation of the proposed diffusional model (Luke et al. 2005). Specifically, such implementation entailed the definition of common biophysics and biochemical laws and assumptions, namely molecular diffusion (Mereghetti et al. 2011) and collision resolution (Figure 1A), as a basic means to guarantee that agent movement complied with the Brownian motion of the molecules (Figure 1B).

The simulation of Brownian motion (ie random-walk motion) is known to follow a square root law involving the average displacement over time and the diffusion coefficient. For the sake of computational tractability, the simulation did not portray the reaction medium (eg water molecules or other molecules that might be part of the laboratorial experiment) as explicit agents. The random motion naturally emerged from collisions between the agents, granted that the velocity of the molecules was consistent with molecular size and environmental constants, such as the temperature and viscosity of the simulated reaction medium.

Simulations were executed on a computer with an Intel (University of Vigo) CPU I7 860 @ 2.80 GHz and 8 GB of RAM DDR3 @ 1,333 MHz CL9 running Windows (University of Vigo, Ourense) 10 64 bits.

Mathematical model of diffusion in a multicellular environment and statistical analysis

The proposed ABM was validated against an algebraic approach for the simplest simulation scenarios, where one *P. aeruginosa* cell was facing a *C. albicans* cell. Similar to the computational model, the mathematical model considered a realistic representation of the cells in terms of size and shape, as well as the perpendicular movement of AHLs in relation to the surface of the *P. aeruginosa* cells. Since no individual molecules were considered in the mathematical model, the correlation between both models was achieved by calculating the surface area of *P. aeruginosa* that, when a plane was projected perpendicularly to the surface of the cell, was still able to intersect the *C. albicans* cell (see Supplemental materials 1 and 2).

The results of the mathematical model were compared against the average of six replicates obtained for each computational simulation. The one-sample Wilcoxon test, a non-parametric alternative test to the one-sample *t*-test, supported this analysis. The goal was to compare a measure of central tendency of the population under observation (here, the median) with a given theoretical value. This test was considered adequate because the size of the sample was small and it does not require the population to be normally distributed. The significance level was set to 5% ($p < 0.05$).

Results

The initial results obtained from the ABM simulations highlighted the importance of cell distance over AHL collision with *C. albicans* (Figure 2). Such importance was also quantified mathematically. Supplemental material 1 details the algebraic determination of the equation that correlated the percentage of AHL molecules expected to reach the *C. albicans* cell when the *P. aeruginosa* cell was horizontally aligned with the *C. albicans* cell (in an imaginary x-axis). The final equation was as follows (Equation 3):

$$\frac{A_{sup}}{A_{total}} = \frac{r_1 r_2 \left(r_1 + r_2 + d - \sqrt{\left(r_1 + r_2 + d\right)^2 - r_1^2} \right)}{\left(r_1 + r_2 + d\right)^2 \left(2r_2 + h\right)} \quad (3)$$

where A_{sup}/A_{total} represents the ratio of area in the *P. aeruginosa* cell, which contributed to AHL molecules that will theoretically collide with the *C. albicans* cell, $r1$ and $r2$ are the radii of *C. albicans* and *P. aeruginosa* cells respectively, h represents the height of the *P. aeruginosa* cell, and d is the distance between the two cells.

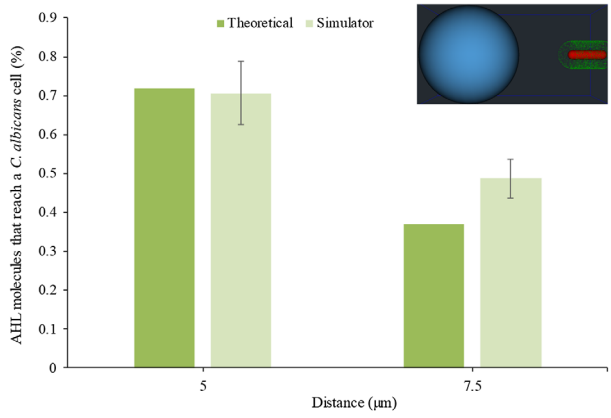

Figure 2. Results for cell distance simulations. The dark green bar shows the theoretical result obtained by the mathematical model. The light green bar shows simulation results, including the SD of the six simulation replicates. The percentage of AHL molecules obtained *in silico* is calculated by counting the number of molecules that reached a *C. albicans* cell and dividing by the total number of AHL molecules in the simulation. A small schematic of the simulated scenario is presented in the top right corner.

Simulation results confirmed that the percentage of AHL molecules reaching the *C. albicans* cell depended on the distance between the two cells, ie the closer the *P. aeruginosa* cell was to the *C. albicans* cell, the more AHL molecules reached the *C. albicans* cell. Differences between the results obtained in the ABM simulations and by the mathematical model were statistically significant ($p < 0.05$) when the distance between *P. aeruginosa* and *C. albicans* was 7.5 µm, but not when the distance was 5 µm ($p > 0.05$). An illustrative video of these simulations is provided in Supplemental material 2.

The following simulations addressed cell orientation as a factor influencing the percentage of AHL molecules that reached the *C. albicans* cell (Figure 3). More specifically, simulations accounted for three-dimensional representations where *C. albicans* and *P. aeruginosa* cells were aligned along an imaginary y-axis (Figure 3A) and a varied distribution of *P. aeruginosa* cells (Figure 3B–D).

The scenario in Figure 3A was similar to the previous scenario (Figure 2) except for the orientation of the *P. aeruginosa* cell. By considering vertical cell alignment, a significantly higher percentage of molecules was expected to reach *C. albicans*, because the surface of the *P. aeruginosa* cell 'facing' a *C. albicans* cell was larger, and the *P. aeruginosa* cell released AHL molecules in a random perpendicular direction.

At this point, the complexity of the algebraic approach increased significantly (see details in Supplemental material 3). The final equation (Equation 4) was:

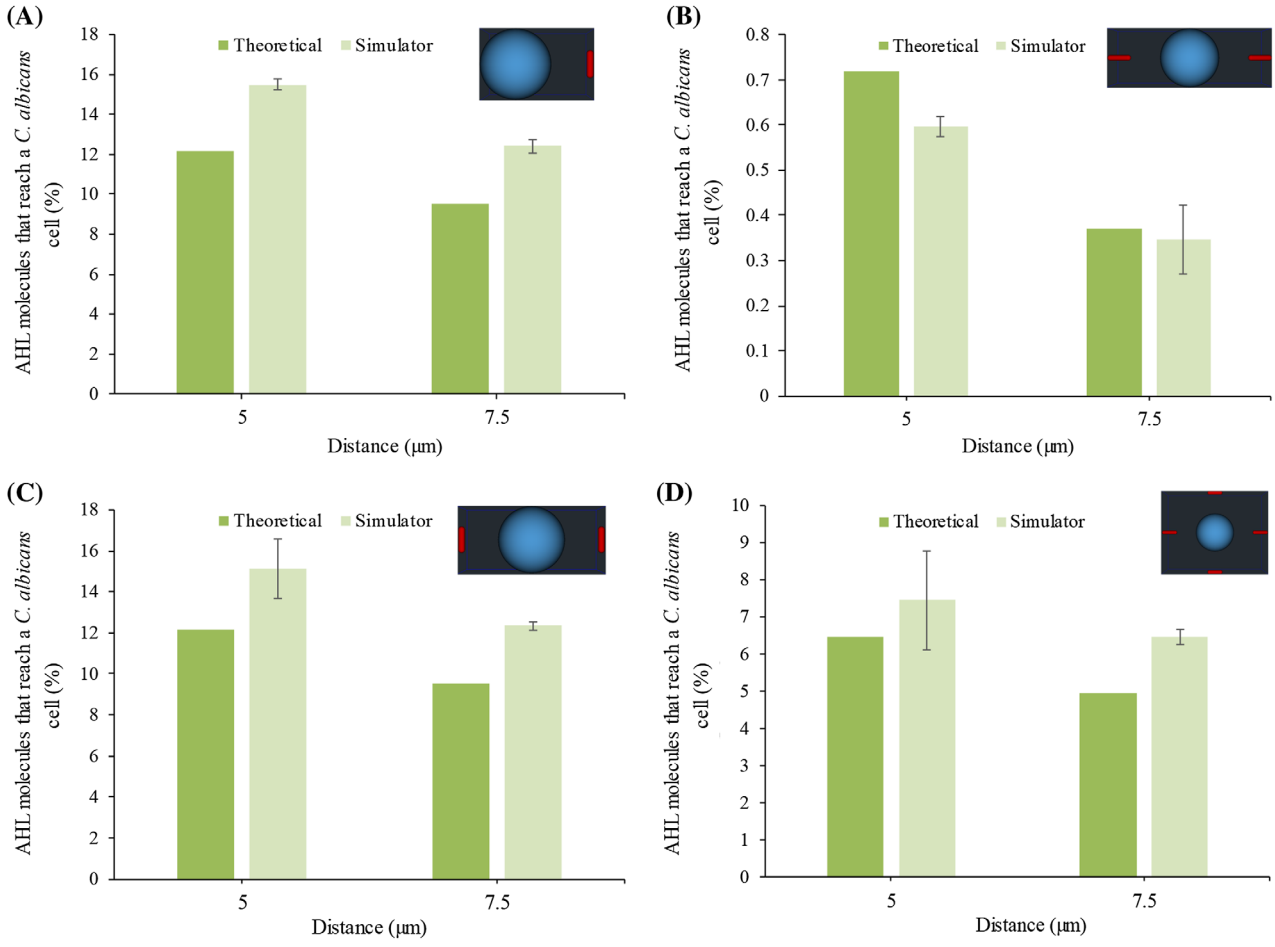

Figure 3. Results for cell orientation and localisation experiments. The dark green bar shows the theoretical results obtained by the mathematical model. The light green bar shows simulation results, including the SD of the six simulation replicates. The percentage of AHL molecules obtained *in silico* is calculated by counting the number of molecules that reached a *C. albicans* cell and dividing by the total number of AHL molecules in the simulation. (A) *P. aeruginosa* positioned vertically to *C. albicans* and both cells are aligned in the x-axis; (B) *P. aeruginosa* cells are positioned horizontal to *C. albicans* and all the cells are aligned in the x-axis; (C) *P. aeruginosa* cells are positioned vertical to *C. albicans* and all the cells are aligned in the x-axis; (D) *P. aeruginosa* cells are positioned vertical and horizontal by pairs to *C. albicans* cells, and cells are aligned in the x- and y-axes. A small schematic of the simulated scenario is presented in the top right corner.

$$\frac{A_{sup}}{A_{total}} = \frac{\frac{hr_2}{2}\left[\arccos\left(\frac{\sqrt{(r_1+r_2+d)^2-r_3^2}}{r_1+r_2+d}\right)+\arccos\left(\frac{\sqrt{(r_1+r_2+d)^2-r_1^2}}{r_1+r_2+d}\right)\right]+\frac{\pi r_3 r_2^2\left((r_1+r_2+d)-\sqrt{(r_1+r_2+d)^2-r_3^2}\right)}{(r_1+r_2+d)^2}}{\pi r_2 h + 2\pi r_2^2} \quad (4)$$

where A_{sup}/A_{total} is the ratio of area in the *P. aeruginosa* cell, which contributed to the AHL molecules that will theoretically collide with the *C. albicans* cell, $r1$ and $r2$ are the radii of *C. albicans* and *P. aeruginosa* respectively, h represents the height of the *P. aeruginosa* cell, $r3$ is the radius of the circumference in *C. albicans* for a height $h/2$, and d is the distance between *C. albicans* and *P. aeruginosa*. In this case, the differences observed between ABM simulations and the mathematical model were statistically significant for both distances ($p < 0.05$).

The simulation of the scenario in Figure 3B was expected to provide results similar to those obtained for the horizontal cell alignment, ie while localisation was similar, the number of *P. aeruginosa* cells was two times greater than the one considered in the previous scenario. Therefore, the percentage of AHL molecules, ie the number of molecules that reached the *C. albicans* cell over the total number of AHL molecules in the simulation, was nearly the same. No statistically significant differences were observed between ABM simulations and the

mathematical model ($p > 0.05$). The same behaviour was assumed for the scenarios in Figure 3A and C, regarding vertical cell alignment and, this time, statistically significant results were obtained for both distances ($p < 0.05$).

The simulation of the scenario in Figure 3D, which considered *P. aeruginosa* cells surrounding a *C. albicans* cell, accounted for different surfaces of a *P. aeruginosa* cell 'facing' a *C. albicans* cell. Since this scenario was a merge of the scenarios illustrated in Figure 3B and C, it was expected to output results in accordance with the 'average' of the results of these previous scenarios. Specifically, the differences observed between ABM simulations and the mathematical model were statistically significant when *P. aeruginosa* was at a 7.5 μm distance from *C. albicans*, but not when the distance was 5 μm ($p > 0.05$). The largest differences observed between computational and algebraic results were <4%. Supplemental material 4 shows the statistical analysis of the results.

Unlike the algebraic approach, ABM simulations were also able to report the time taken by individual AHL molecules to reach the *C. albicans* cell. For instance, when both cells were separated by 7.5 μm, most AHL molecules reached *C. albicans* within 72–80 μs, but a fraction of the molecules took longer, typically those molecules released from the more distant sections of the *P. aeruginosa* cell (Figure 4). Considering the scenarios from A to E, the mean average time obtained was 79 μs, the shortest time was 72 μs (ie the time taken by the molecules closer to *C. albicans*) and the longest time was 104 μs (ie the time taken by the molecules at the longest distance).

Figure 4F illustrates the results obtained during the simulation of a higher number of bacterial cells, clustered together in groups of three. Here, the concentration of AHL molecules in certain areas of the environment was significantly greater, which typically led to the occurrence of more collisions among the molecules. As a result, the number of AHLs reaching *C. albicans* was less predictable. The number of AHLs colliding with *C. albicans* reached its highest at 72 μs, but a peak was observed again after 116 μs. The mean average time taken by AHLs to reach *C. albicans* was 91 μs, the shortest time was 72 μs and the longest time was 236 μs.

Environment feeding simulations were used to further describe the production of AHL molecules by other cells in the multicellular environment (Figure 5), ie the effect of cell vicinity (Figure 5A) and the overall distribution of the cell population (Figure 5B) in the time taken by *C. albicans* to reach the QS threshold. As stated earlier, while a pure mathematical approach is possible for the simplest scenarios, the complexity of the calculations increases considerably for scenarios of this complexity, because molecules collide among themselves and higher deviations will naturally occur.

The proposed ABM is able to address such complexity by simply describing the environment, the agents (including varying localisation) and the rules of behaviour. When observing cell vicinity (Figure 5A), deviations caused by molecular collisions (ie changes in trajectory) were expected to occur. Likewise, when looking into the effect of the whole cell population (Figure 5B), the random distribution of the cells was expected to be the major cause of difference between theoretical and simulation results.

Finally, the most complex scenario accounted for a multicellular environment containing several *C. albicans* and *P. aeruginosa* cells encased in a 3-D matrix, ie a biofilm. Biofilms are a mix of seemingly unarranged cells in a matrix of extracellular polymeric substances, with micro channels that carry nutrients and other compounds. Therefore, the rationale for simulating this scenario was that, depending on the spatial location, *C. albicans* would be variably exposed to AHL molecules and this could help explain why the phenotypic switching of individual *C. albicans* cells in a biofilm typically occurs at different time points.

The proposed model enabled the representation of the spatial arrangements with more than one *C. albicans* cell and the prediction of morphological transition in individual *C. albicans* cells. Specifically, simulations assumed that all *P. aeruginosa* cells released the same amount of AHL molecules (ie 5,000 molecules per cell), and the threshold for morphological transition (ie the amount of AHL molecules needed to inhibit hyphal transition) would be the same for all *C. albicans* cells. As shown in Figure 6, only *Candida* A was expected to undergo morphological transition, since the number of AHL molecules that collided with *Candida* B did not reach the hypothesised threshold of 2,000 molecules in 200 μs.

Discussion

The first generation of biofilm models were continuum models with a focus on population and resource dynamics that described biofilms as a one-dimensional homogeneous layer (Moustaid et al. 2013; Langebrake et al. 2014). More recently, the spatial heterogeneous structure of biofilms was addressed in multi-dimensional models. Various mathematical modelling techniques have been applied, namely stochastic individual-based models (Müller et al. 2006; Hong et al. 2007), stochastic cellular automata models (Pizarro et al. 2004; Chambless and Stewart 2007; Machineni et al. 2017), deterministic differential equation models (Frederick et al. 2011; Schroeder et al. 2015; Rahman et al. 2015) and hybrid models (Weber and Buceta 2013). While using different approaches, all these models share complexity as their major limitation (Emerenini et al. 2015).

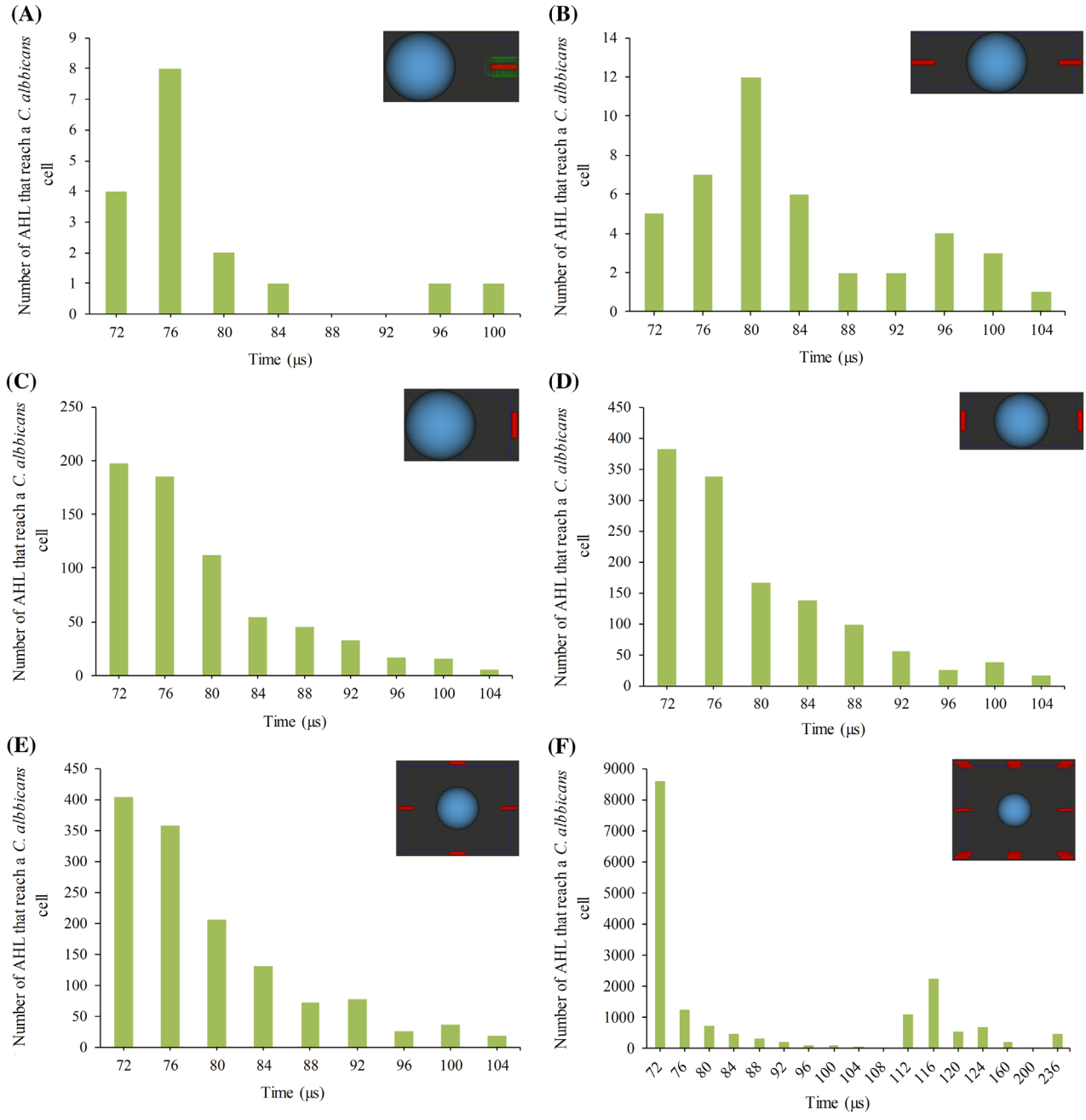

Figure 4. Histograms of the average time taken by AHL molecules to move from *P. aeruginosa* to *C. albicans* cells in cell localisation simulations. All histograms denote a positive skew. The distance between the cells is 7.5 μm. (A) *P. aeruginosa* is positioned horizontal to *C. albicans* and both cells are aligned in the x-axis; (B) *P. aeruginosa* cells are positioned horizontal to *C. albicans* and all the cells are aligned in the x-axis; (C) *P. aeruginosa* is positioned vertical to *C. albicans* and both cells are aligned in the y-axis; (D) *P. aeruginosa* cells are positioned vertical to *C. albicans* and all the cells are aligned in the y-axis; (E) *P. aeruginosa* cells are positioned vertical and horizontal by pairs to *C. albicans* and the cells are aligned in the x- and y-axes; (F) *P. aeruginosa* cells are positioned in groups of three surrounding *C. albicans*. A small schematic of the simulated scenario is presented in the top right corner.

Several modelling alternatives introduced simplifying assumptions in an attempt to minimise model complexity. For instance, some QS models assumed discrete QS states or simplified the relationship between intracellular and extracellular signal concentrations, while others assumed the existence of concentration thresholds for QS behaviour (Chopp et al. 2002; Müller et al. 2006; Netotea et al. 2009; Matur et al. 2015). Further models treated extracellular molecular concentration as a parameter, and studied the response of a single cell. For example, some works studied cell robustness to various sources of noise and the existence of bistability at the single-cell level (Fagerlind et al. 2003; Anguige et al. 2006; Müller and Uecker 2013). However, single cell models are still not

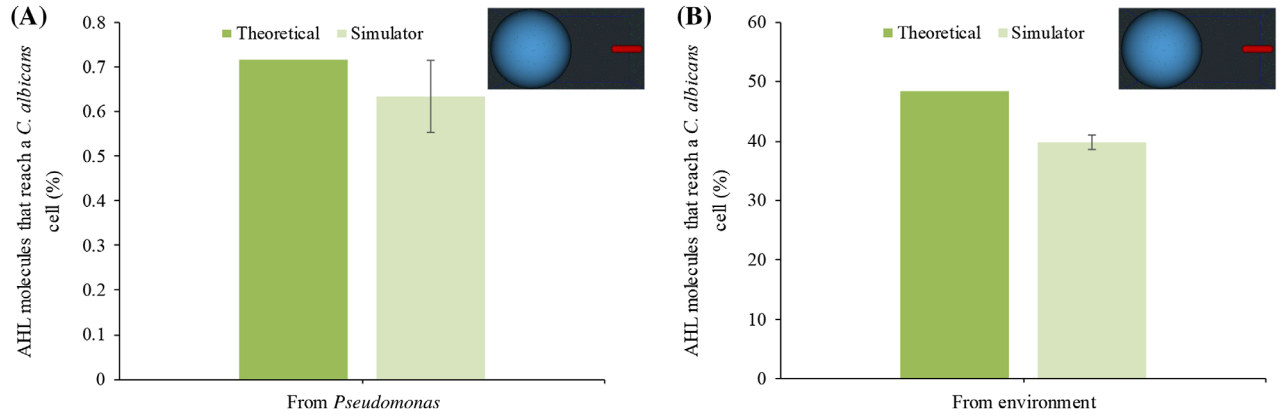

Figure 5. Results for environment feeding simulations. (A) Percentage of AHL molecules that reach *Candida* from *Pseudomonas* cells; (B) percentage of AHL molecules that reach *Candida* from the environment. The dark green bar shows the theoretical results obtained by the mathematical model. The light green bar shows simulation results, including the SD of the six simulation replicates. The distance between the cells is 5 µm. A small schematic of the simulated scenario is presented in the top right corner.

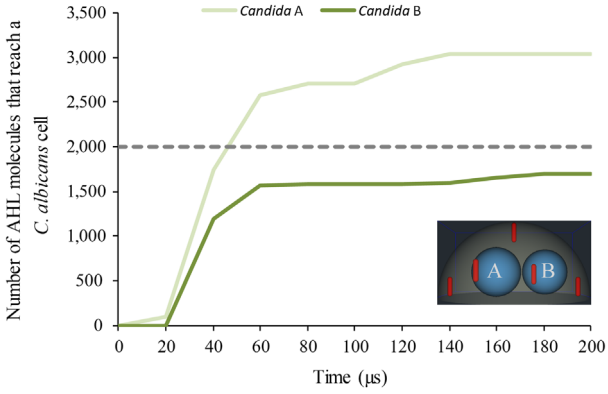

Figure 6. Results for biofilm simulations. The light and dark green lines show simulation results for two *C. albicans* cells exposed to AHL molecules at different rates. The grey dashed line represents the imaginary threshold for morphological conversion. A small schematic of the simulated scenario is presented at the bottom right corner.

capable of fully depicting QS functions at the population level (Brown 2013). Therefore, efforts have been made to model molecular and population processes collectively, ie treat cells as discrete entities and track the molecular dynamics separately within each cell (Garcia-Ojalvo et al. 2004; Goryachev et al. 2005; Melke et al. 2010; Uecker et al. 2014). Although providing the most detailed and realistic representation, the mathematical and computational complexity of these models prevents full exploration of the process dynamics (Pérez-Velázquez et al. 2016).

The present work shows, for the first time, the potential of ABM to understand biofilm dynamics at the single-cell and single-molecule levels. One of the main advantages of the ABM approach when compared with algebraic models and other existing models is a reduction in model complexity, which enables the practical simulation of more realistic biological scenarios (Fozard et al. 2012; Emerenini et al. 2015). Notably, ABM enables the simulation of multiple scenarios of cell spatial distribution, and thus the observation of the impact that cell location has in molecular diffusion and, consequently, in QS communication. Moreover, these models are also able to describe the trajectory of individual molecules, and hence obtain spatial and temporal information at the single-molecule level. These data can be more easily validated by direct comparison with single particle tracking experiments, as well as provide detailed information on the behaviour of more complex scenarios involving multiple cells in a seemingly random distribution.

In the present study of AHL diffusion in a mixed-species multicellular environment, a pure mathematical approach could be applied to the simplest scenarios, but, as expected, the complexity of the calculations hindered its use in more elaborate scenarios. Mathematical complexity escalated when the number of cells and molecules increased, because more diffusion and collision phenomena had to be considered. However, the proposed ABM was able to address such complex situations by simply describing the environment, the agents (including varying localisation) and the rules of behaviour. Specifically, the ABM enabled the comparison of different cell populations (in terms of both cell number and distribution) as well as track AHL molecules from the moment they were secreted by *P. aeruginosa* until the moment they reached *C. albicans*.

The computational and mathematical models provided similar results, differing by no more than 4% in the whole spectrum of scenarios studied. Molecular collisions (and implicitly changes in trajectory), the physical dimensions of the AHL molecules, and the initial random distribution of AHL molecules, are three of the possible causes for the observed differences.

In terms of assumptions, the proposed model considered that cells are static and that only *P. aeruginosa* released the AHL molecules that contributed to altering the cell morphology of *C. albicans*. In reality, quite a few molecules contribute to these morphological changes. One such molecules is farnesol, that is released by *C. albicans* itself (Méar et al. 2013; Mallick and Bennett 2013). Moreover, in multicellular environments such as biofilms, cells are continuously adhering and sloughing, and even inside the biofilm structure cells demonstrate a certain level of movement (Flemming et al. 2016). In spite of the simplistic assumption, the ABM model enabled the observation of the impact that cell location and distance have over morphological switching. In the future, as experimental methods advance and further tracking of particles becomes possible, the ABM model may be refined and improved in order to model alternative scenarios, such as *C. albicans* internal signalling *via* farnesol molecules. It may also be used to assess the effect that changes in the location and concentration of molecules and cells will have on very similar biofilms.

Acknowledgements

The SING group thanks CITI (Centro de Investigación, Transferencia e Innovación) from University of Vigo for hosting its IT infrastructure. The authors also acknowledge that M. Pérez-Pérez and G. Pérez-Rodríguez were supported by pre-doctoral fellowships from the Xunta de Galicia.

Disclosure statement

No potential conflict of interest was reported by the authors.

Funding

This work has been funded by a Research Grant 2014 by the European Society of Clinical Microbiology and Infectious Diseases (ESCMID) to AL; the Portuguese Foundation for Science and Technology (FCT) [grant numbers UID/BIO/04469/2013, UID/EQU/00511/2013] units and COMPETE 2020 [grant numbers POCI-01-0145-FEDER-006684, POCI-01-0145-FEDER-006939]; North Portugal Regional Operational Programme (NORTE 2020) [grant number NORTE-01-0145-FEDER-000005 – LEPABE-2-ECO-INNOVATION] under the Portugal 2020 Partnership Agreement, through the European Regional Development Fund (ERDF).

ORCID

Nuno F. Azevedo http://orcid.org/0000-0001-5864-3250
Anália Lourenço http://orcid.org/0000-0001-8401-5362

References

Alberghini S, Polone E, Corich V, Carlot M, Seno F, Trovato A, Squartini A. 2009. Consequences of relative cellular positioning on quorum sensing and bacterial cell-to-cell communication. FEMS Microbiol Lett.292:149–161. [accessed 2017 Sep 6]. http://www.ncbi.nlm.nih.gov/pubmed/19187204. doi:10.1111/fml.2009.292.issue-2.

Anguige K, King JR, Ward JP. 2006. A multi-phase mathematical model of quorum sensing in a maturing *Pseudomonas aeruginosa* biofilm. Math Biosci. 203:240–276. [accessed 2017 Mar 7]. http://linkinghub.elsevier.com/retrieve/pii/S0025556406000915. doi:10.1016/j.mbs.2006.05.009.

Brown D 2013. Linking molecular and population processes in mathematical models of quorum sensing. Bull Math Biol. 75:1813–1839. [accessed 2017 Mar 7]. http://link.springer.com/10.1007/s11538-013-9870-1.

Carnes EC, Lopez DM, Donegan NP, Cheung A, Gresham H, Timmins GS, Brinker CJ. 2010. Confinement-induced quorum sensing of individual *Staphylococcus aureus* bacteria. Nat Chem Biol. 6:41–45. http://www.ncbi.nlm.nih.gov/pubmed/19935660. doi:10.1038/nchembio.264.

Chambless JD, Stewart PS. 2007. A three-dimensional computer model analysis of three hypothetical biofilm detachment mechanisms. Biotechnol Bioeng. 97:1573–1584. [accessed 2017 Mar 7]. http://doi.wiley.com/10.1002/bit.21363. doi:10.1002/(ISSN)1097-0290.

Chopp DL, Kirisits MJ, Moran B, Parsek MR. 2002. A mathematical model of quorum sensing in a growing bacterial biofilm. J Ind Microbiol Biotechnol. 29:339–346. [accessed 2017 Mar 7]. http://link.springer.com/10.1038/sj.jim.7000316.

Emerenini BO, Hense BA, Kuttler C, Eberl HJ. 2015. A mathematical model of quorum sensing induced biofilm detachment. PLoS ONE. 10:e0132385. doi:10.1371/journal.pone.0132385.

Fagerlind MG, Rice SA, Nilsson P, Harlén M, James S, Charlton T, Kjelleberg S. 2003. The role of regulators in the expression of quorum-sensing signals in *Pseudomonas aeruginosa*. J Mol Microbiol Biotechnol. 6:88–100. [accessed 2017 Mar 7]. http://www.ncbi.nlm.nih.gov/pubmed/15044827. doi:10.1159/000076739.

Feig M, Sugita Y. 2013. Reaching new levels of realism in modeling biological macromolecules in cellular environments. J Mol Graph Model. 45:144–156. http://www.pubmedcentral.nih.gov/articlerender.fcgi?artid=3815448&tool=pmcentrez&rendertype=abstract. doi:10.1016/j.jmgm.2013.08.017.

Flemming H-C. 1993. Biofilms and environmental protection. Water Sci Technol. 27. [accessed 2017 Jun 19]. http://wst.iwaponline.com/content/27/7-8/1.

Flemming H-C, Wingender J, Szewzyk U, Steinberg P, Rice SA, Kjelleberg S. 2016. Biofilms: an emergent form of bacterial life. Nat Rev Microbiol. 14:563–575. doi:10.1038/nrmicro.2016.94.

Fourie R, Ells R, Swart CW, Sebolai OM, Albertyn J, Pohl CH 2016. *Candida albicans* and *Pseudomonas aeruginosa* interaction, with focus on the role of eicosanoids. Front Physiol. 7:64.

Fozard Ja, Lees M, King JR, Logan BS. 2012. Inhibition of quorum sensing in a computational biofilm simulation. Biosystems. 109:105–114. doi:10.1016/j.biosystems.2012.02.002.

Frederick MR, Kuttler C, Hense BA, Eberl HJ. 2011. A mathematical model of quorum sensing regulated EPS production in biofilm communities. Theor Biol Med Model. 8:8. [accessed 2017 Mar 7]. http://tbiomed.biomedcentral.com/articles/10.1186/1742-4682-8-8.

Gao M, Zheng H, Ren Y, Lou R, Wu F, Yu W, Liu X, Ma X. 2016. A crucial role for spatial distribution in bacterial quorum sensing. Sci Rep. 6:7819. [accessed 2017 Sep 6]. http://www.nature.com/articles/srep34695. doi:10.1038/srep34695.

Garcia-Ojalvo J, Elowitz MB, Strogatz SH. 2004. Modeling a synthetic multicellular clock: repressilators coupled by quorum sensing. Proc Natl Acad Sci USA. 101:10955–10960. [accessed 2017 Mar 7]. http://www.pnas.org/cgi/doi/10.1073/pnas.0307095101.

Goryachev AB, Toh D-J, Wee KB, Lee T, Zhang H-B, Zhang L-H. 2005. Transition to quorum sensing in an Agrobacterium population: a stochastic model. PLoS Comput Biol. 1:e37. [accessed 2017 Mar 7]. http://dx.plos.org/10.1371/journal.pcbi.0010037.

Hogan DA, Vik A, Kolter R. 2004. A *Pseudomonas aeruginosa* quorum-sensing molecule influences *Candida albicans* morphology. Mol Microbiol. 54:1212–1223. [accessed 2017 Jun 5]. http://doi.wiley.com/10.1111/j.1365-2958.2004.04349.x.

Hong D, Saidel WM, Man S, Martin JV. 2007. Extracellular noise-induced stochastic synchronization in heterogeneous quorum sensing network. J Theor Biol. 245:726–736. [accessed 2017 Mar 7]. http://linkinghub.elsevier.com/retrieve/pii/S0022519306005662. doi:10.1016/j.jtbi.2006.12.006.

Kalwarczyk T, Tabaka M, Holyst R. 2012. Biologistics – diffusion coefficients for complete proteome of *Escherichia coli*. Bioinformatics. 28:2971–2978. [accessed 2016 Nov 2]. http://www.ncbi.nlm.nih.gov/pubmed/22942021. doi:10.1093/bioinformatics/bts537.

Karupiah G, Chaudhri G. 2004. Immunology, infection, and immunity. Immunol Cell Biol. 82:651–651. doi:10.1111/imcb.2004.82.issue-6.

Klis FM, de Koster CG, Brul S. 2014. Cell wall-related bionumbers and bioestimates of *Saccharomyces cerevisiae* and *Candida albicans*. Eukaryot Cell. 13:2–9. doi:10.1128/EC.00250-13.

Langebrake JB, Dilanji GE, Hagen SJ, De Leenheer P. 2014. Traveling waves in response to a diffusing quorum sensing signal in spatially-extended bacterial colonies. J Theor Biol. 363:53–61. [accessed 2017 Mar 7]. http://linkinghub.elsevier.com/retrieve/pii/S0022519314004457. doi:10.1016/j.jtbi.2014.07.033

Luke S, Cioffi-Revilla C, Panait L, Sullivan K, Balan G. 2005. MASON: a multiagent simulation environment. Simul Trans Soc Model Simul Int. 81:517–527. http://sim.sagepub.com/cgi/doi/10.1177/0037549705058073.

Machineni L, Rajapantul A, Nandamuri V, Pawar PD. 2017. Influence of nutrient availability and quorum sensing on the formation of metabolically inactive microcolonies within structurally heterogeneous bacterial biofilms: an individual-based 3D cellular automata model. Bull Math Biol. 79:594–618. [accessed 2017 Mar 7]. http://link.springer.com/10.1007/s11538-017-0246-9.

Mallick EM, Bennett RJ. 2013. Sensing of the microbial neighborhood by *Candida albicans*. Heitman J, editor. PLoS Pathog. 9:e1003661. [accessed 2017 Mar 7]. http://dx.plos.org/10.1371/journal.ppat.1003661.

Matur MG, Müller J, Kuttler C, Hense BA. 2015. An approximative approach for single cell spatial modeling of quorum sensing. J Comput Biol. 22:227–235. [accessed 2017 Mar 7]. http://online.liebertpub.com/doi/10.1089/cmb.2014.0198.

Méar J-B, Kipnis E, Faure E, Dessein R, Schurtz G, Faure K, Guery B. 2013. *Candida albicans* and *Pseudomonas aeruginosa* interactions: more than an opportunistic criminal association? Med Mal Infect. 43:146–151. [accessed 2017 Mar 7]. http://linkinghub.elsevier.com/retrieve/pii/S0399077X13000528. doi:10.1016/j.medmal.2013.02.005.

Melke P, Sahlin P, Levchenko A, Jönsson H. 2010. A cell-based model for quorum sensing in heterogeneous bacterial colonies.Shvartsman S, editor. PLoS Comput Biol. 6:e1000819. [accessed 2017 Mar 7]. http://dx.plos.org/10.1371/journal.pcbi.100081910.1371/journal.pcbi.1000819.

Mereghetti P, Kokh D, McCammon JA, Wade RC. 2011. Diffusion and association processes in biological systems: theory, computation and experiment. BMC Biophys. 4:2. [accessed 2018 Feb 26]. http://bmcbiophys.biomedcentral.com/articles/10.1186/2046-1682-4-2.

Moustaid F El, Eladdadi A, Uys L. 2013. Modeling bacterial attachment to surfaces as an early stage of biofilm development. Math Biosci Eng. 10:821–842. [accessed 2017 Mar 7]. http://www.aimsciences.org/journals/displayArticlesnew.jsp?paperID=8473. doi:10.3934/mbe.

Müller J, Kuttler C, Hense BA, Rothballer M, Hartmann A. 2006. Cell-cell communication by quorum sensing and dimension-reduction. J Math Biol. 53:672–702. [accessed 2017 Mar 7]. http://link.springer.com/10.1007/s00285-006-0024-z.

Müller J, Uecker H. 2013. Approximating the dynamics of communicating cells in a diffusive medium by ODEs-homogenization with localization. J Math Biol. 67:1023–1065. [accessed 2017 Mar 7]. http://link.springer.com/10.1007/s00285-012-0569-y.

Netotea S, Bertani I, Steindler L, Kerényi A, Venturi V, Pongor S. 2009. A simple model for the early events of quorum sensing in *Pseudomonas aeruginosa*: modeling bacterial swarming as the movement of an "activation zone&quot. Biol Direct. 4:6. [accessed 2017 Mar 7]. http://biologydirect.biomedcentral.com/articles/10.1186/1745-6150-4-6.

Peleg AY, Hogan DA, Mylonakis E. 2010. Medically important bacterial-fungal interactions. Nat Rev Microbiol. 8:340–349. doi:10.1038/nrmicro2313.

Pérez-Rodríguez G, Gameiro D, Pérez-Pérez M, Lourenço A, Azevedo NF. 2016. Single molecule simulation of diffusion and enzyme kinetics. J Phys Chem B. 120:3809–3820. [accessed 2016 Nov 2]. http://pubs.acs.org/doi/abs/10.1021/acs.jpcb.5b12544.

Pérez-Velázquez J, Golgeli M, García-Contreras R. 2016. Mathematical modelling of bacterial quorum sensing: a review. Bull Math Biol. 78:1585–1639. [accessed 2018 Feb 26]. http://www.ncbi.nlm.nih.gov/pubmed/27561265.

Pizarro GE, García C, Moreno R, Sepúlveda ME. 2004. Two-dimensional cellular automaton model for mixed-culture biofilm. Water Sci Technol. 49:193–198. [accessed 2017 Mar 7]. http://www.ncbi.nlm.nih.gov/pubmed/15303741.

Rahman KA, Sudarsan R, Eberl HJ. 2015. A mixed-culture biofilm model with cross-diffusion. Bull Math Biol. 77:2086–2124. [accessed 2017 Mar 7]. http://link.springer.com/10.1007/s11538-015-0117-1.

Schroeder JL, Lunn M, Pinto AJ, Raskin L, Sloan WT. 2015. Probabilistic models to describe the dynamics of migrating microbial communities. Zhou Z, editor. PLoS ONE. 10:e0117221. [accessed 2017 Mar 7]. http://dx.plos.org/10.1371/journal.pone.0117221.

Stiegelmeyer SM, Giddings MC. 2013. Agent-based modeling of competence phenotype switching in *Bacillus subtilis*. Theor Biol Med Model. 10:23. doi:10.1186/1742-4682-10-23.

Sudbery PE. 2011. Growth of *Candida albicans* hyphae. Nat Rev Microbiol. 9:737–748. doi:10.1038/nrmicro2636.

Trejo-Hernández A, Andrade-Domínguez A, Hernández M, Encarnación S. 2014. Interspecies competition triggers virulence and mutability in *Candida albicans-Pseudomonas aeruginosa* mixed biofilms. ISME J. 8:1974–1988. doi:10.1038/ismej.2014.53.

Trovato A, Seno F, Zanardo M, Alberghini S, Tondello A, Squartini A. 2014. Quorum *vs.* diffusion sensing: a quantitative analysis of the relevance of absorbing or reflecting boundaries. FEMS Microbiol Lett. 352:198–203. [accessed 2017 Sep 6]. http://www.ncbi.nlm.nih.gov/pubmed/24484313. doi:10.1111/fml.2014.352.issue-2.

Tsimring LS. 2014. Noise in biology. Reports Prog Phys. 77:26601. [accessed 2018 Feb 26]. http://www.ncbi.nlm.nih.gov/pubmed/24444693.

Uecker H, Uecke H, Müller J, Hense BA. 2014. Individual-based model for quorum sensing with background flow. Bull Math Biol. 76:1727–1746. [accessed 2017 Mar 7]. http://link.springer.com/10.1007/s11538-014-9974-2.

Weber M, Buceta J. 2013. Dynamics of the quorum sensing switch: stochastic and non-stationary effects. BMC Syst Biol. 7:6. [accessed 2017 Mar 7]. http://bmcsystbiol.biomedcentral.com/articles/10.1186/1752-0509-7-6.

Winson MK, Camara M, Latifi A, Foglino M, Chhabra SR, Daykin M, Bally M, Chapon V, Salmond GP, Bycroft BW. 1995. Multiple N-acyl-L-homoserine lactone signal molecules regulate production of virulence determinants and secondary metabolites in Pseudomonas aeruginosa. Proc Natl Acad Sci USA. 92:9427–9431. doi:10.1073/pnas.92.20.9427.

Yu J. 2014. Coordination and control inside simple biomolecular machines. Adv Exp Med Biol. 805:353–384. doi:10.1007/978-3-319-02970-2.